Hindawi
Journal of Nanomaterials
Volume 2022, Article ID 9378487, 11 pages
https://doi.org/10.1155/2022/9378487

Research Article

Surface Roughness Evaluation in Turning of Nimonic C263 Super Alloy Using 2D DWT Histogram Equalization

S. Lakshmana Kumar,[1] **M. Thenmozhi**,[2] **R. M. Bommi**,[3] **Chakaravarthy Ezilarasan**,[4] **V. Sivaraman**,[5] **and Sivaprakasam Palani**[6]

[1]*Department of Mechanical Engineering, Sona College of Technology, Salem, India*
[2]*Department of Computer Science, Sona College of Arts and science, Salem, India*
[3]*Institute of ECE, Saveetha School of Engineering, SIMATS, Chennai, India*
[4]*Center for Applied Research, Chennai Institute of Technology, Chennai, India*
[5]*Department of Mechanical Engineering, Dr. N.G.P. Institute of Technology, Coimbatore, India*
[6]*Department of Mechanical Engineering, College of Electrical and Mechanical Engineering, Addis Ababa Science and Technology University, Addis Ababa, Ethiopia*

Correspondence should be addressed to S. Lakshmana Kumar; lakshmana@gmail.com and Sivaprakasam Palani; shiva@aastu.edu.et

Received 24 February 2022; Accepted 9 April 2022; Published 28 April 2022

Academic Editor: V. Vijayan

Surface roughness of specimens is an important area of research since it influences the performance of machined parts. Meanwhile, employing a vision system to judge the roughness of the machined surface of specimens via captured images acquired from the specimen is an innovative and extensively used method. In this investigation, a vision system is used to capture the SEM images of the machined surface. The two-dimensional images of the machined surface of the Nimonic263 alloy are used to approximate the profile of the surface of specimens in finish turning. Surface roughness was detected in simulated images of specimens in a variety of machining conditions using the imaging technology. In this research work, the surface texture is extracted using a technique that combines 2D surface images and wavelet transform approach. The 2D wavelet transform has the capability to disintegrate a machined surface image into multiresolution depiction for several surface characteristics and can be utilized for surface evaluation. The difference in the histogram frequency of an illuminated region of interest (ROI) from turned surface images was analyzed to aid in the evaluation of surface roughness with an average prediction error of less than 3.2%.

1. Introduction

In the production and development of industrial parts, both the microstructure of the surface on a μm-scale and integrity strongly influence the characteristics and functions of components, such as wear, precision, anticorrosion, fitting, friction, and antifatigue attributes. Direct methods and indirect methods are the two types of techniques available for surface roughness evaluation. Using a toolmaker's microscope, 3D surface profiler, optical microscope, or SEM (offline method) or a CCD camera, significant procedures evaluate the surface profile of machined surfaces. These observing systems are often based on a comparison of an optimum cutting process reference signal with the actual process signal [1, 2]. Electrical discharge machining was recently used to machine Nimonic super alloy (EDM) [3]. The measurement scale (L) and root mean squared roughness (Rq) are determined to comprehend the surface property based on scaling analysis [4]. Researchers have developed a method to determine the degree of tool wear by evaluating the machined surfaces' texture using an image processing methodological approach to the image of the machined surface to overcome these limitations. Tool wear measurement, surface quality control, workpiece surface

texture measurements, and other machining processes can all benefit from digital image processing (DIP) with machine vision. Image processing techniques were used to determine the surface roughness of large-scale SEM images [5, 6].

Response surface methodology (RSM) was employed to do mathematical modelling of surface roughness and flank wear. ANOVA is assessing the impact of each individual parameter on responses. Between the simulated and experimental data, there was a maximum inaccuracy of 13% and 7% in flank wear and roughness of the surface, respectively [7]. Machining of Nimonic alloy and Inconel alloy is regarded as critical, and it is necessary to investigate the impact of machining factors on machining responses in order to identify the best machining/control factors and their levels in order to improve the machined surface's integrity/machinability [8–10]. The majority of image processing-based machined surface roughness evaluation approaches depend on feature extraction processes [11].

A review of tool condition monitoring based on image processing approaches was presented by Dutta et al. The findings of Dutta et al. suggest that in a single experimental setup, direct approaches will be employed to validate the outcomes of indirect procedures. The tool wear was evaluated based on the workpiece's rough surface. The gray-level cooccurrence matrix (GCLM) is an efficient technique for selecting the best texture based on entropy metric [12]. Shahabi and Ratnam [13] proposed surface roughness evaluation by capturing the images of the machined surface in cycle using computer vision in this investigation. Grayscale imaging was used to detect simulated pictures of specimens in a variety of machining conditions. The results demonstrated that this method may be utilized to mimic and analyze a specimen's surface profile in finish lathe machining as a tool tip fingerprint.

Dutta et al. [14] designed an improvised GLCM algorithm to monitor the tool condition with an offset parameter. According to the findings, the GLCM analysis focussed on the pixel pair spacing (PPS) value selection that is entirely reliant on the variances of feed marks having been turned [15]. Using response surface methodology, the impact of drilling parameters like tool rotational speed, geometrical parameters, flank wear, and feed rate on surface roughness was investigated. GLCM-based texture analysis of workpiece surface images was employed to obtain waviness information through spatial correlation of pixels [16]. DWT-based texture analysis has also been used to machine surface images to gather information on modification in surface texture due to the increase in tool flank wear via Ga, GRMS, and energy in space-frequency localization.

Liu et al. [17] investigated the explored flank face surface texturing on the WC/Co carbide tools with various geometrical features. The tools with microscale grooves parallel to the primary cutting edge on the flank face had the best flank wear resistance. The tool wear was assessed using the DWT method on machined surface images [18]. The DWT was used to perform a microscale study of a turned surface with average coefficient of determination values of 0.957 and 0.953, respectively; an exponential association of GRMS and energy values with progressing flank wear of the tool is discovered. Illumination-compensated pictures were suggested by John and Arunachalam to evaluate the surface roughness of turned surfaces in the grinding process [19].

Gandla et al. investigated surface roughness using incremental forming [20]. Taylor Hobson Talysurf is used to measure the surface roughness of manufactured parts, which varies from 0.61 to 3.61 mm. Few images were acquired from each formed part and saved in an image dataset for machine vision-based surface roughness evaluation. The wavelet transform method, Euclidean distance method, and Hamming distance approach were used to classify these images into three classes predicated on the range of surface roughness. The wavelet-based technique has a maximum classification performance of 95.4 percent, according to the results. The classifying effectiveness of the Hamming and Euclidian distance approaches is 78.39 percent and 81.48 percent, respectively. Ali and Dhar [21] proposed an ANN technique for forecasting surface roughness in turning. This model may be used to optimize the cutting process for efficient and economical manufacturing by predicting tool wear and surface roughness in the turning process. CNN algorithms have gained popularity in the assessment of surface roughness in recent years [22–25]. Because feature extraction is included into the network during the convolution phase, this technique eliminates it. Five loss functions are selected and evaluated for the prediction models based on their potential application and accuracy. The actual and expected surface roughness values are compared using a stylus-based profilometer.

The vibration and communication particle swarm optimization (VCPSO) algorithm, developed by Xu et al., included self-random vibration and interparticle communication processes [26]. When estimating tool wear, the ANFIS learned by the VCPSO algorithm (ANFIS-VCPSO) outperformed other intelligent models. The VCPSO algorithm was tested using benchmark functions, and the results showed that it is capable of global optimization. All the while, the VCPSO algorithm was used to determine the best milling parameter combinations under a variety of tool wear conditions. The technique proposed in this article extracts the surface texture by combining two-dimensional surface photography and a wavelet approach. Then, the future surface roughness is predicted by extracting the time delay parameters, the embedding dimension, and the false nearest neighbour of the produced surface texture. All offline and online approaches can estimate surface roughness parameters based on evidence from the surface image [27]. The stylus tracing (ST) technique became the most widely known way of evaluating the surface properties of components in recent decades, due to the implementation of tactile profilometers [24, 25]. The ST involves measuring the texture of the surface and calculating the R_a roughness parameter but in contact with the surface. The noncontact approach provided in this work, on the other hand, can predict surface texture and roughness characteristics more precisely and with less prediction error by using DWT histogram equalization and Laplacian filtering. This technology represents a significant advancement in the development of smart surface roughness measuring devices that may be used in the smart manufacturing sector in the near future.

2. Experimental Setup

In this experiment, a super alloy Nimonic C263 workpiece was machined in dry cutting mode with CBN inserts. After cutting the entire length of the workpiece, the machined surfaces were imaged as 640 × 480-pixel gray-level image data using a CCD camera connected to a personal computer with machine vision capacity at 5 different locations on the surface of the workpiece. The photos were taken with a diffused lighting setup online. With relation to the workpiece, the camera and lighting source were put in place. For the most part, the illumination source was managed to hold at a 30-degree angle. The average flank wear of the insert (V_B average) was also determined using a Leica S6D microscope at 10 magnification and Leica QWin-V3 image capturing software.

Simultaneously, the surface roughness of the turned surface (R_a) was measured at the appropriate locations, where R_a stands for average surface roughness. Table 1 summarises the cutting conditions of turning operations performed on Nimonic 263. For each of the machining conditions, three sets of experiments were carried out (as listed in Table 1). Table 2 summarises the camera setup and surface roughness tester specifications. Each image was cropped to 210 × 210 pixels before processing. The MATLAB® environment was used for all image processing (version 7.8.0.347 R2021).

2.1. Materials. Nimonic C263 alloy with 150 mm length and 70 mm diameter with hardness of 32 HRc was considered the work material. It is a material with good resistance to high temperature and oxidation owing to its Ni, Cr, and cobalt content. The following are the chemical components of the workpiece material (in % weight): 0.48 Al, 2.94 Ti, 0.15 W, 0.04 Nb, 0.02 C, 0.02 V, 0.007 Ta, 0.001 S, 0.19 Si, 52.49 Ni, 20 Cr, 0.46 Mn, 0.07 Cu, 6.29 Mo, 16.7 Co, 1.0 Fe, 0.48 Al, and 1.94 Ti.

2.2. Methods. The experimental study was carried out on a NAGMATI175 lathe. Figures 1(a)–1(d) show the experimental setup, insert, tool holder, and flank wear. The Sandvik makes Cubic Boron Nitride (CBN) inserts to the specifications of CNGA 120 408S01030A, 7025 grade was chosen as the insert for the tests, and a PCLNR 2020 K12 tool holder was being used to fix the insert. Back rake angle (BRA) (6°), side rake angle (SRA) (6°), end relief angle (ERA) (6°), side relief angle (SRA) (6°), end cutting edge angle (ECEA) (5°), side cutting angle (SCEA) (5°), and nose radius (NR) (0.8 mm) are the tool signatures of the insert. The cutting parameter's effect on surface roughness in turning the Nimonic C-263 alloy was investigated. All turning trials were carried out by a new cutting edge. The experiment was carried out using an L_9 orthogonal array. The machining factors such as feed rate, cutting speed, and depth of cut were considered, and their ranges are listed in Table 3.

A tool maker's microscope was used to measure the surface roughness offline at regular intervals. The measuring range is X-200 mm and Y-100 mm, the microscope stand tilting range is 12, the maximum distance between centres is 700 mm, the maximum diameter accommodating between centres is 100 mm, the plane stage area is260 mm × 270 mm, and the resolution is 0.2 lm (linear) (1 minute). Table 4 shows the L_9 orthogonal array and surface roughness measured using conventional and unconventional methods.

Table 1: Machining Nimonic C263—experimental setup.

Machine tool	NAGMATI175: lathe *H*: 165 mm *S*: 305 mm Speed: 54–1200 rpm Feed: 0.048–0.716 mm/rev Power: 1 HP
Insert	PVD-coated carbide insert
Cutting speed	80 m/min, 125 m/min, 195 m/min
Feed	0.055 mm/rev, 0.096 mm/rev, 0.159 mm/rev
Depth of cut	0.25 mm, 0.50 mm, 0.75 mm

Table 2: Machining Nimonic C263—imaging setup.

Equipment	Specifications
Scanning electron microscopy	Imaging module: 17" touch screen monitor rotary knob, magnification range: 120x to 24,000x
Surface roughness tester	Cutoff: 0.8 mm Filter: Gauss l: 0.8 mm Evaluation "l": 4.00 mm Measuring speed: 0.5 mm/s

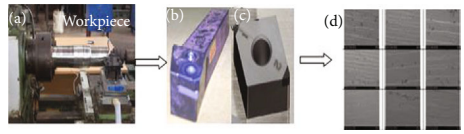

Figure 1: (a) Experimental setup, (b) tool holder, (c) insert, and (d) SEM image of flank wear.

Table 3: Machining parameters and assigned levels.

S. no	Factors	Unit	*L1*	*L2*	*L3*
1	Speed (*S*)	mm/rev	0.055	0.096	0.159
2	Feed (*F*)	m/min	80	125	195
3	Depth of cut (a_p)	mm	0.25	0.50	0.75

3. Methodology

Machine vision systems by default initiate with the image acquisition stage. Machine vision-based methods are extremely recommended for safe evaluation in in situ investigation of machined surfaces. Turned surface images are captured utilizing a high-end vision camera to evaluate the surface texture. The machine vision camera acquires the machined surface images after turning operation, to examine the surface texture. The captured machined surface images undergo normalization to cope up with lighting changes that might affect the image quality. The overall process is encapsulated in the block diagram as shown in Figure 2.

Table 4: L_9 orthogonal array, experimental trail results, and unconventional method results.

Exp. trail no.	Coded values			Actual setting values			Surface roughness (experimental values) (R_a)	Unconventional measured values (R_a)
	S	F	a_p	S	F	a_p		
1	1	1	1	80	0.055	0.25	3.3057	1.25
2	1	2	2	80	0.096	0.50	3.55	1.75
3	1	3	3	80	0.159	0.75	2.43	2.10
4	2	1	2	125	0.055	0.50	4.89	1.50
5	2	2	3	125	0.096	0.75	3.77	1.10
6	2	3	1	125	0.159	0.25	2.73	1.50
7	3	1	3	195	0.055	0.75	0.844	1.075
8	3	2	1	195	0.096	0.25	2.27	0.90
9	3	3	2	195	0.159	0.50	3.65	0.85

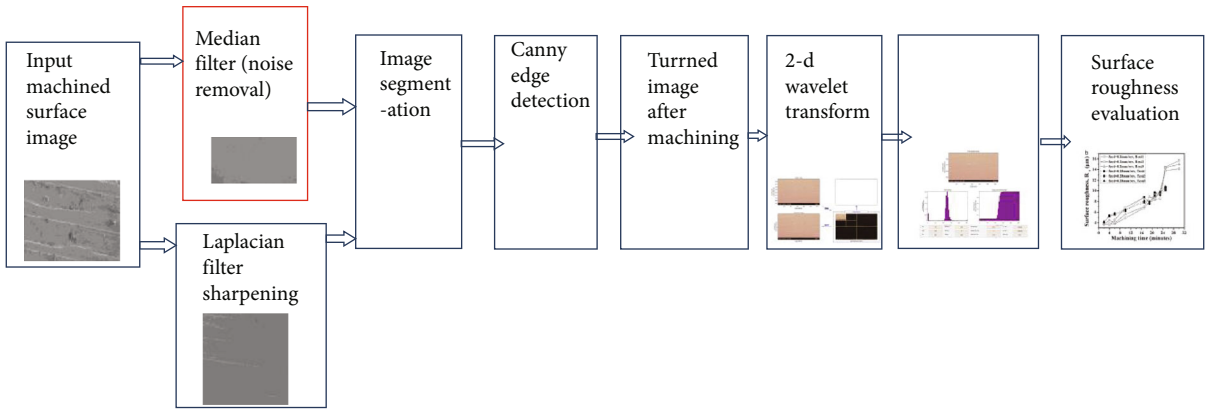

Figure 2: DWT histogram equalization.

Normalization is performed as given below:

$$s(m,n) = \frac{r(p,q) - \min(r)}{\max(r) - \min(r)} * 255. \quad (1)$$

The normalized image matrix is represented by $s(m,n)$. The intensity of each pixel in the image matrix is represented by $r(p,q)$. The image matrix's minimum and maximum pixel intensity values are denoted as min (r) and max (r), respectively. The machined surface images obtained after turning operation at varied cutting conditions had an enormous flank wear resulting in variation in workpiece textures. This increased flank wear (V_B) reduces the cutting insert noise radius, which affects the machined surface. Machine vision system-refined machined surface images contain flaws such as nanoparticle settlings and feed marks.

The digital camera output is

$$p(m,n) = b(m,n) + \varepsilon(m,n), \quad (2)$$

where $b(m,n)$ is the original image and $\varepsilon(m,n)$ is the added noise.

Wiener filtering is utilized to retrieve the images $b(m,n)$ disrupted by noise.

$$\lambda = \frac{1}{MN} \sum_{p_1,p_2 \in p} b(p_1,p_2), \quad (3)$$

where λ is the local mean intensity surrounding every pixel. Also, p denotes M-by-N neighborhood of every pixel, and $b(p_1,p_2)$ is the location of every pixel in the local neighborhood mask p. Also, variance of intensity surrounding every pixel is obtained by

$$\sigma^2 = \frac{1}{MN} \sum_{p_1,p_2 \in p} b^2(p_1,p) - \lambda^2. \quad (4)$$

The Wiener filter reduces the noise depending upon the statistical variables by lowering the variance of the neighboring pixels. In stage 3, the image segmentation is performed to segment the object from its surrounding pixels. This is utilized to set the cutting tool pixel intensity to 0 and the background to 1; it is explained in the below equation:

$$f_1(m,n) = \{1 \text{ if } f(m,n) \geq T, 0 \text{ if } f(m,n\} \leq T\}, \quad (5)$$

Table 5: Machining parameters to examine the effect of surface roughness.

Lathe machine	Nagamathi lathe machine
Specimen	Nimonic C263
Cutting speed	498 m/min
Feed rate	0.1 mm/rev
Time	5, 7, and 9 min
Cooling agent	Air
Depth of cut	0.2 mm

where $f(m, n)$ denotes the actual image of the tool tip after noise removal in the algorithm step 2 and $f_1(m, n)$ denotes the tool tip image after segmenting the cutting tool image. Also, T is the threshold value set by default utilizing the MATLAB command. The machine details and machining conditions considered for the study are given in Table 5.

Preprocessing is required to improve image quality through contrast stretching, histogram equalization, noise reduction through filtering, and inhomogeneous illumination compensation, among other things. Low-pass filtering (median filter) is very effective at reducing noise in machined surface images, particularly cutting tool images, because noise can occur due to dirt, oils, and precision machining dust and dirt on the surface of an object. The Laplacian filter is a second-order temporal high-pass filter that is used to sharpen machined surface images so that the feed marks can be seen clearly. The segmentation method and feature extraction are carried out after preprocessing. By calculating the image gradient and direction, the feature extraction ensures the information of the edges of the workpiece surface images. Because of its noise immunity and ability to detect actual edges with minimal flaws, the Canny edge detector is used in the field of machine vision. Convolution is performed between both the machined surface image and a Gaussian smoothing filter with a standard deviation of s in the Canny edge identification technique. The gradient computation for the smoothened image is the next step. This technique can be used to fetch the edges of a workpiece surface texture. To capture turned images with good contrast, a dispersed lighting prototype such as fibre optic-guided light with a DC-regulated light source and infrared interference filter is used. Segmentation is the process of dividing an image into multiple sections according to a set of rules. The feature-state method collects pixel characteristics into feature vectors, which are then used to assign pixels to classes by selecting a threshold value. Because the 2D wavelet transform can disintegrate a workpiece surface impression into multiresolution depictions for several surface morphologies, it can be used to evaluate surfaces. Signal vectors derived from feed mark images are used to represent the image's grayscale intensity. Use the 2D wavelet transform and the key local intensity variation technique to decompose the image signal vector. Wavelet transform is a time-frequency-conversion mathematical procedure that is frequently used. The frequency analysis of the signal into scalar analysis is dealt with by wavelet analysis.

$$\Phi_{i,j}(y) = \frac{1}{\sqrt{i}}\varphi\left[\frac{y-j}{i}\right], \tag{6}$$

where i seems to be the scale parametric quantity for varying frequency and "j" is the interpretation parametric quantity and $i, j(x)$ is the wave function. Surface roughness is an important parameter for evaluating and controlling manufacturing quality because it can affect the friction coefficient, creep life, and fatigue strength of a machined part. Surface roughness results due to enhanced tool wear; it serves as an indication to replace the tool. Surface roughness evaluation procedures based on image processing can be performed online through E-evaluation. However, this facility is not available in traditional procedures. A rough surface tends to scatter more quantity of light. This causes larger dark regions to form that result in decrease in the image signal RMS value. A rough surface ends up with huge speckle patches that in turn reduce the variance, within the fixed evaluation length. The histogram mapping of an illuminated area of interest (ROI) from machined surface photographs was studied to see if there was any fluctuation in histogram frequency, which helps with surface roughness evaluation [28].

3.1. Evaluation Parameters. The roughness average, also known as the arithmetic average height (R_a), is a roughness parametric parameter that is often used in quality control.

$$R_a = \frac{1}{N}\sum_{i=1}^{N}|y_i|. \tag{7}$$

"N" is the number of samples for a certain evaluation duration and y_i denotes how far the profile deviates from the average line. The root mean square slope (R_{dq}) and arithmetic mean slope (R_{da}) hybrid parametric quantities are used.

$$R_{da}, \text{Arithmetic Mean Slope} = \sum_{i=1}^{N}\frac{|\delta i|}{N}. \tag{8}$$

δ_i is the slope at point "i" and "N" is the total number of points.

$$R_{dq}, \text{Root Mean Square Slope} = \sqrt{\sum_{i=1}^{N}\frac{\delta i^2}{N}}. \tag{9}$$

4. Results and Discussion

4.1. Characterization of the Machined Surface Utilizing Image Histogram. The surface profile of the workpiece surface is used to measure surface roughness in this paper. The MATLAB software is used to create an intensity

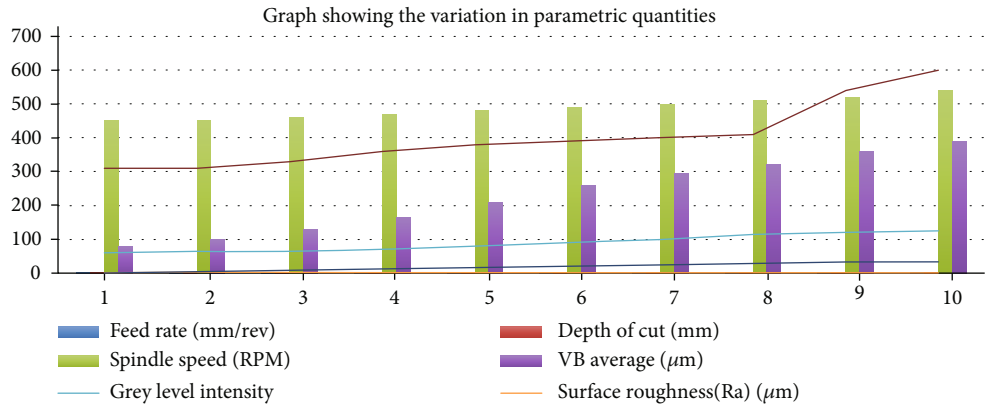

Figure 3: Graphical representation of the variations in parametric quantities.

Table 6: Evaluation parameters in DWT histogram equalization.

Feed rate (mm/rev)	Depth of cut (mm)	Spindle speed (rpm)	V_B average (μm)	Gray-level intensity	Surface roughness (R_a) (μm)	Machining time (minutes)	Histogram frequency (Hz)
0.05	0.25	450	80	60	1.25	0	310
0.07	0.50	450	100	65	1.75	4	310
0.2	0.75	460	130	65	2.10	8	330
0.25	0.75	470	165	70	1.50	12	360
0.26	0.25	480	210	80	1.10	16	380
0.28	0.50	490	260	90	1.50	20	390
0.28	0.50	500	295	100	1.075	24	400
0.28	0.75	510	320	115	0.90	28	410
0.28	0.25	520	360	120	0.85	32	540
0.28	0.25	540	390	125	0.5	33	600

histogram for the workpiece surface image. The histogram is a visual representation of how the intensity of gray levels increases as the surface quality of the machined surface changes. The left portion of histogram denotes small intensity values, and the right portion denotes larger intensity values. The machined metal surface has high reflectivity; hence, it is convenient to monitor the right side of the histogram. Therefore, gray level of 125 is taken as the reference to evaluate the number of histogram frequency. The reflectivity is enhanced if the machined surface is smooth, thereby resulting in greater frequency values. The histogram for the machined surface is obtained by taking the gray-level intensity values on the x-axis and surface roughness R_a values taken on the y-axis. The machined surface is smooth possessing a surface roughness value of $R_a = 0.5\,\mu$m and gray-level intensity of 125, at a frequency of 600 Hz. In the second case, the machined surface is coarse possessing a surface roughness value of $R_a = 1.075\,\mu$m and gray-level intensity value of 100 at a frequency of 400 Hz. By analyzing the histogram of the machined surface image, it enables one to determine if a given machine surface is coarse or smooth. The work involves observing and inspecting the machined surface while turning the Nimonic 263 material with coated carbide inserts at various spindle speeds and feed combinations. Variations in the histogram statistical characteristics that aid in evaluating the surface finish were explored in the histogram form of an illuminated area of interest (ROI) from turning machine surface images. The results clearly show that the turning procedure's cutting specifications have no effect on surface roughness. Figure 3 shows the relationship between machining time and histogram frequency for various feed rates and a steady depth of cut of 0.2 mm at 450 and 510 rpm spindle speeds. The graphs displayed give a general sense of the machined surface's histogram frequency. Only the lowest and maximum feeds at two different speeds are shown in the graphs. Again for entire cutting considerations, the machined surface's surface roughness remains constant. Many investigations have determined that the R_a value changes in a stable range, just as the histogram frequencies of the machined surface obtained with a machine vision system do. The results in Table 6 show that, while the cutting speed and feed rate vary, they have no effect on the machined surface's histogram frequency. For a consistent change in the histogram profile, changing the feed rate causes a change in the form of the feed marks over the machined surface. Various cutting speeds and feed rates were used in the technique.

Figure 4 depicts the original machined surface image and its histogram equivalent. The histogram graph is fetched by taking the surface roughness values on the y-axis and feed rate on the x-axis. An image histogram is a graphical representation of a digital image's tonal distribution. It assigns a

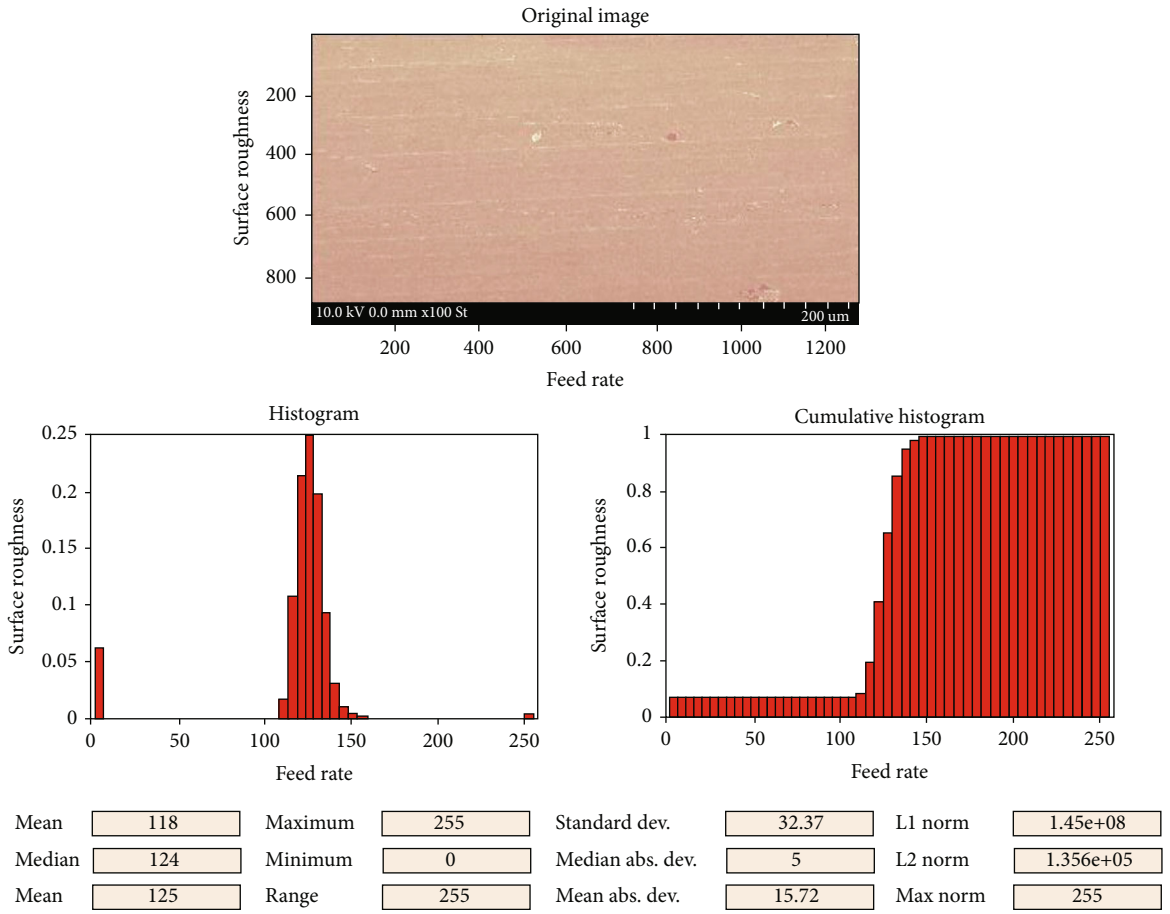

Mean	118	Maximum	255	Standard dev.	32.37	L1 norm	1.45e+08
Median	124	Minimum	0	Median abs. dev.	5	L2 norm	1.356e+05
Mean	125	Range	255	Mean abs. dev.	15.72	Max norm	255

Figure 4: Original image and its histogram equivalent.

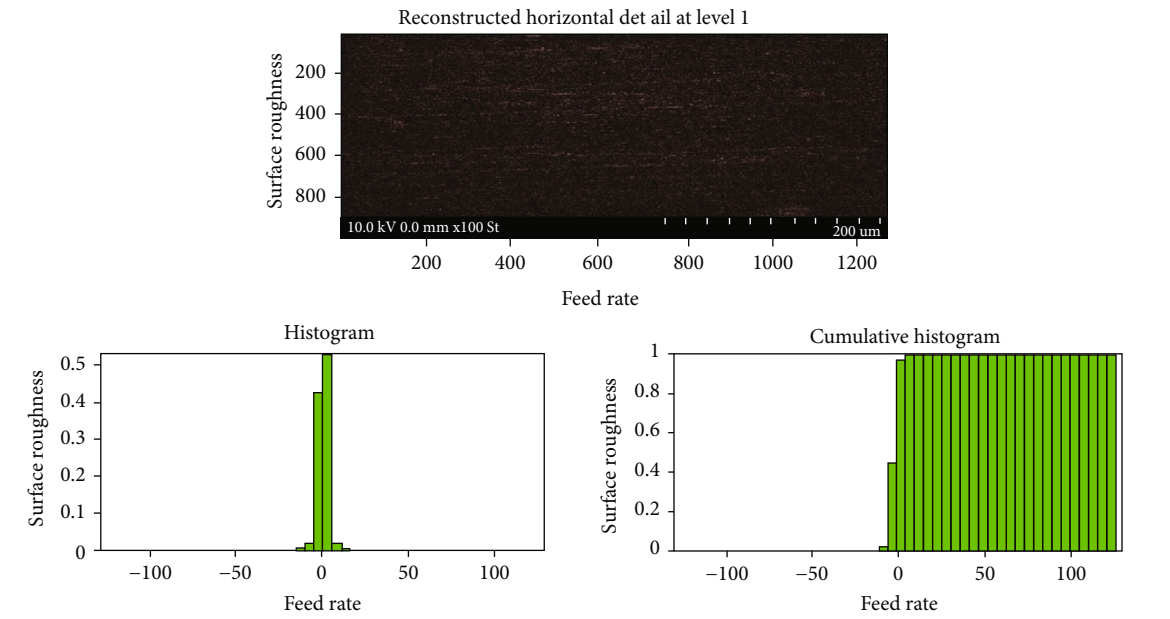

Mean	0	Maximum	127.5	Standard dev.	4.104	L1 norm	2.211e+06
Median	0	Minimum	−127.5	Median abs. dev.	1.25	L2 norm	4550
Mean	2.55	Range	255	Mean abs. dev.	1.8	Max norm	127.5

Figure 5: Reconstructed image and its histogram equivalent.

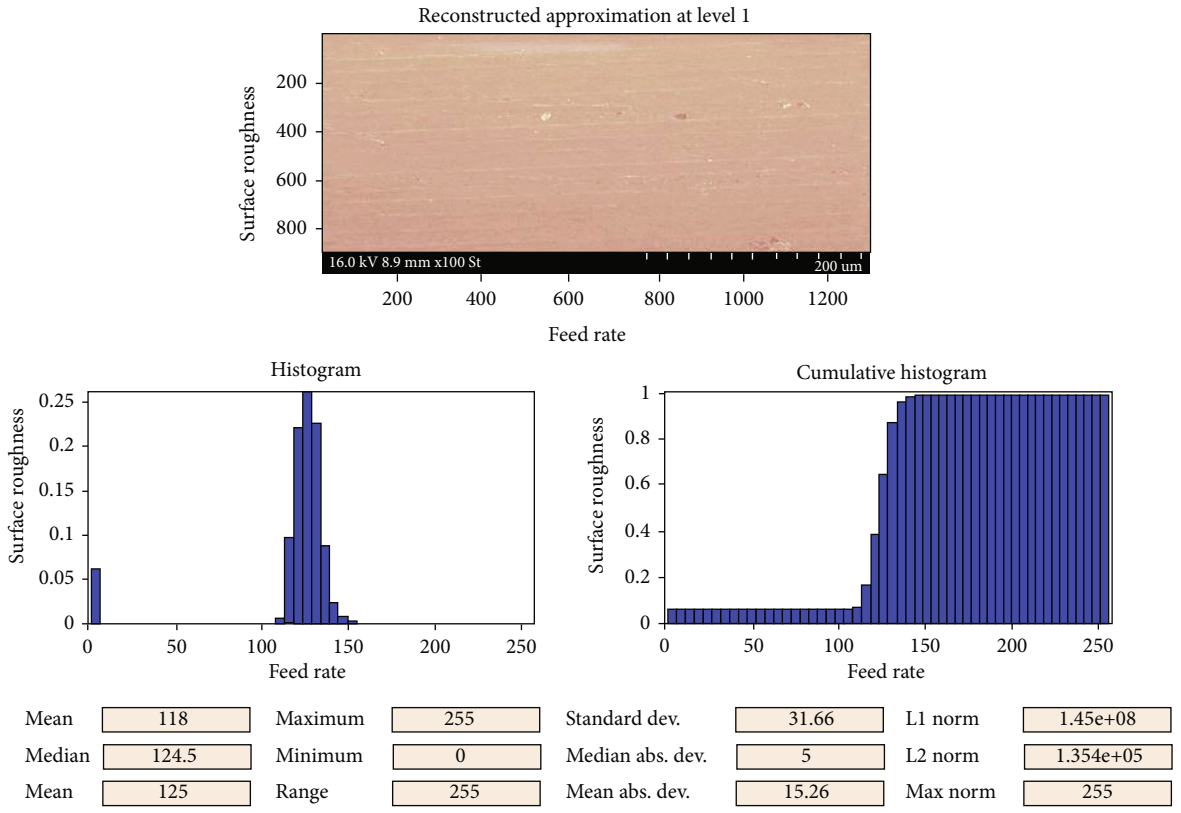

Figure 6: Reconstructed approximation and its histogram.

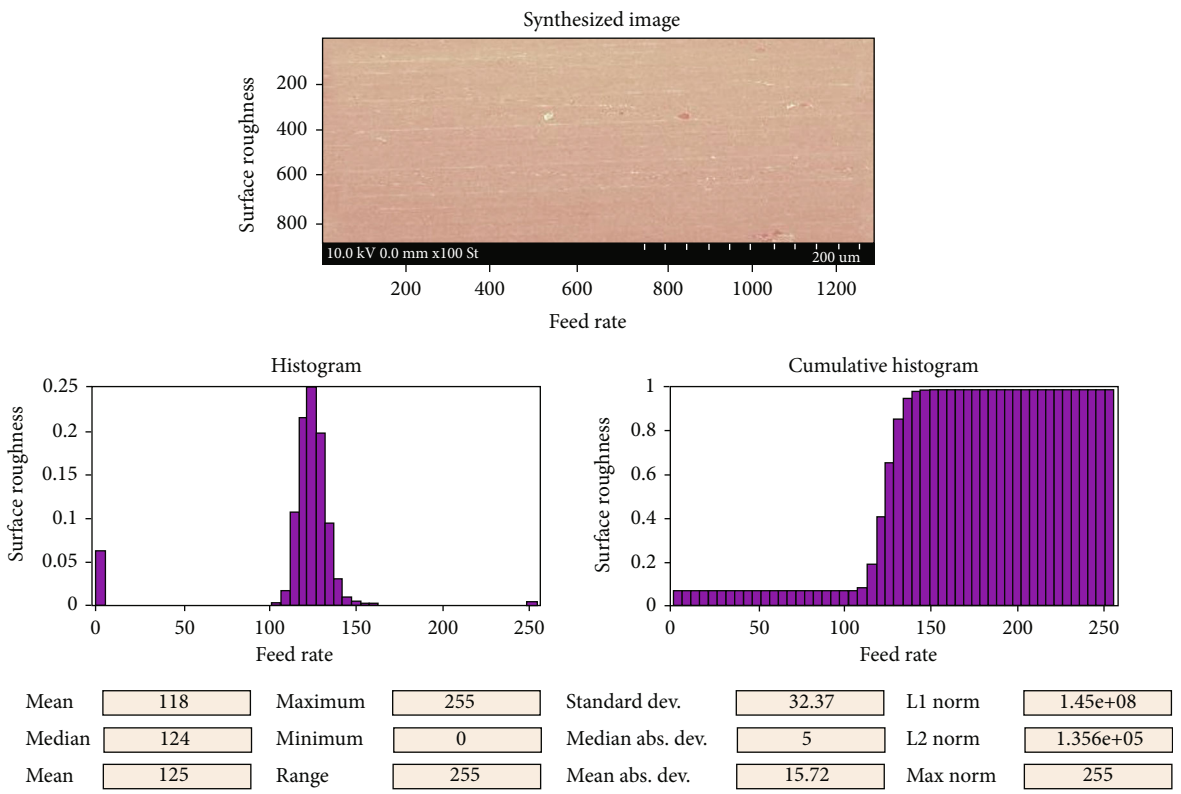

Figure 7: Synthesized image and its histogram equivalent.

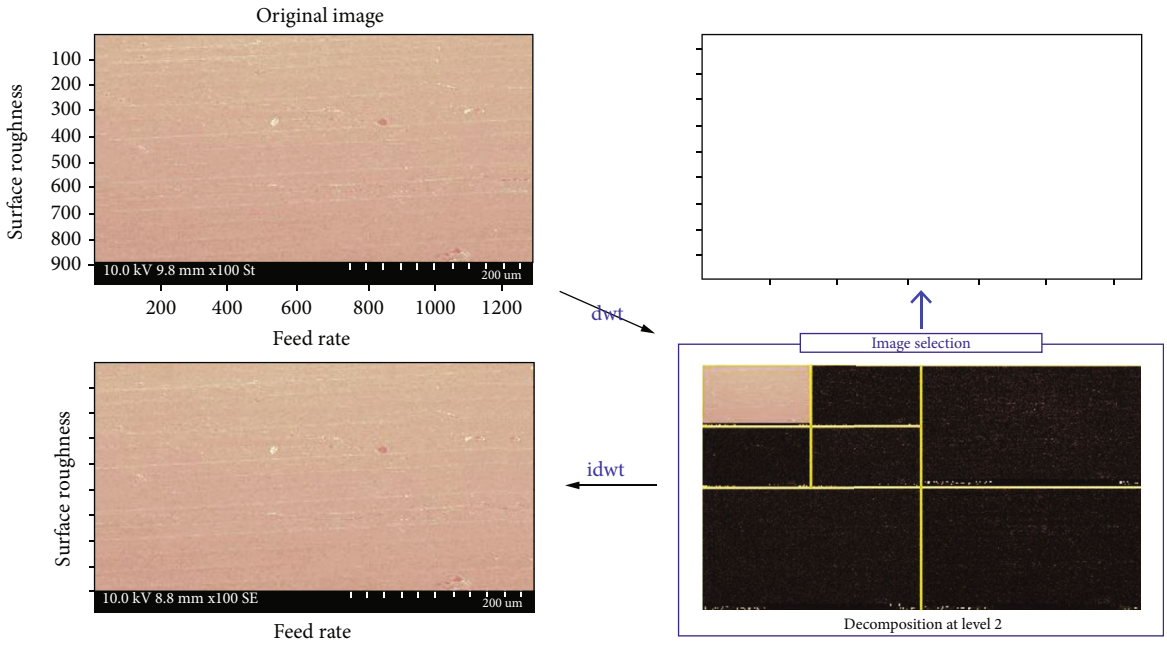

Figure 8: Decomposition using discrete wavelet transform.

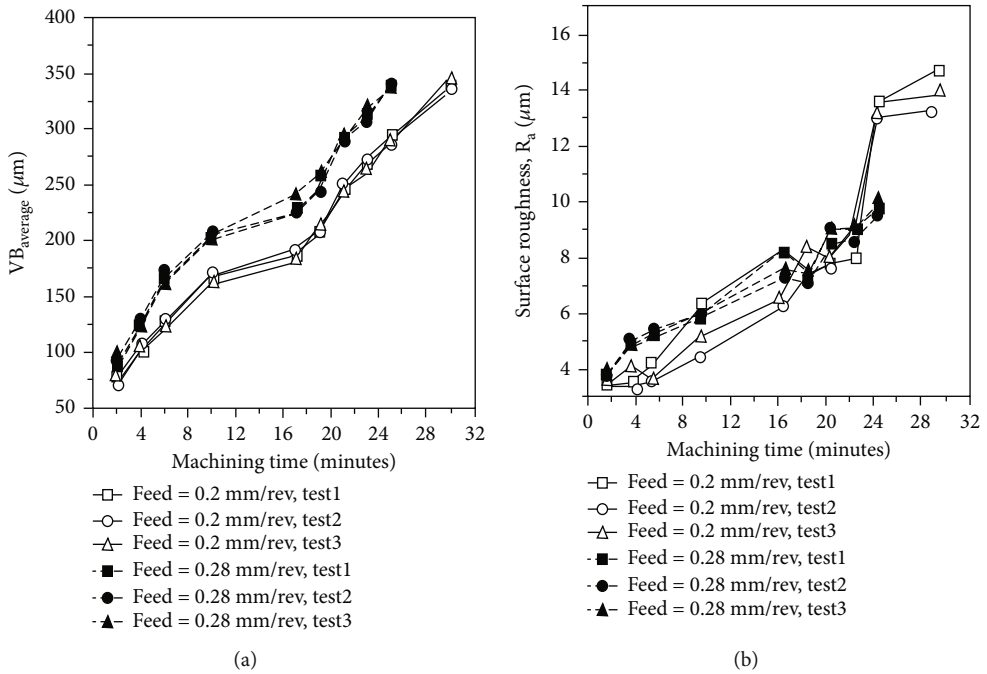

Figure 9: (a) Average flank wear vs. machining time. (b) Average surface roughness (R_a) vs. machining time.

pixel value to each tonal value. A viewer can quickly assess the entire tonal distribution by looking at the histogram for a specific image.

Figure 5 depicts the reconstructed machined surface image and its corresponding histogram equivalent. The histogram graph is fetched by taking the surface roughness values on the y-axis and the feed rate on the x-axis. Image reconstruction is the process of putting together 2D and 3D images from scattered or insufficient data.

Figure 6 depicts the reconstructed approximation at level 1 and its corresponding histogram equivalent. The histogram graph is fetched by taking the surface roughness values on the y-axis and the feed rate on the x-axis. The cumulative histogram is a histogram in which the vertical axis displays not only the number for a single bin but also the number for that bin and all bins with lower response variable values.

Figure 7 depicts the synthesized image at level 1 and its corresponding histogram equivalent. Image synthesis is the

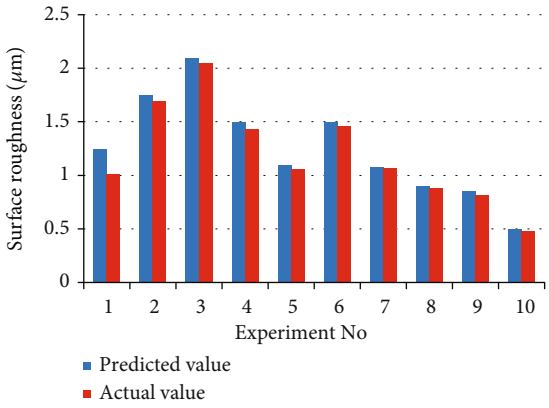

Figure 10: Graph showing the variation in measured and predicted values.

Table 7: Prediction error based on experimental values and DWT histogram equalization.

S. no	Surface roughness (R_a) (μm)		Prediction error
	Predicted value	Measured value	
1	1.25	1.01	3.3057
2	1.75	1.69	3.55
3	2.10	2.05	2.43
4	1.50	1.43	4.89
5	1.10	1.06	3.77
6	1.50	1.46	2.73
7	1.075	1.066	0.844
8	0.90	0.88	2.27
9	0.85	0.82	3.65
10	0.5	0.48	4.16

technique to create novel images from the image specifications. The histogram graph is fetched by taking the surface roughness values on the y-axis and the feed rate on the x-axis.

Figure 8 shows the decomposition of the original machined surface image and the equivalent generated image using discrete wavelet transform (DWT). Image decomposition segregates an input image as structural and textual components.

The average flank wear enhances with cutting time, as depicted in Figure 9(a), and the surface roughness is depicted in Figure 9(b). It demonstrates that, under the similar machining conditions, increasing cutting speed increases flank wear progressively. Higher cutting speeds cause the material to pass away in a short period of time, allowing the machining interface to become an adiabatic system. The cutting tool softens even as temperature increases, resulting in increased tool wear. The influence of feed rate on flank wear was measured using a 498 m/min cutting speed and a 0.1 mm cut depth.

$$\text{Prediction Error} = \frac{\text{Predicted value} - \text{Measured value}}{\text{Measured value}} * 100. \quad (10)$$

The predicted value is obtained by utilizing discrete wavelet transform (DWT) and the measured value from experimental investigation.

As seen in Figure 10 and Table 7 from the above analysis, it is clear that the average prediction error obtained using discrete wavelet transform is 3.16% which is very less when compared to conventional algorithms and techniques.

5. Conclusion

In this research, noncontact surface roughness estimation method has been proposed and investigated. This unconventional method involves steps of noise removal (median filtering), sharpening using the Laplacian filter, image segmentation, Canny edge detection, 2D wavelet transform, and histogram equalization. An improved DWT-combined histogram equalization is used to evaluate the surface roughness with minimum complexity and high accuracy. The following are the significant findings of this experimental study and analysis:

(i) Histogram equalization has been shown to be a reliable method for determining surface roughness

(ii) The proposed method is noncontact, with no additional surface damage to the work item and less complexity than standard surface roughness assessment methods

(iii) Surface texture estimation on machined surfaces is used to verify the effectiveness of the suggested new method

(iv) The results show that this approach predicts surface roughness with a 3.16 percent average prediction error

Abbreviations

SEM: Scanning electron microscopy
CCD: Charge coupled device
EDM: Electrical discharge machining
DIP: Digital image processing
RSM: Response surface methodology
ANOVA: Analysis of variance
GCLM: Gray-level cooccurrence matrix
PPS: Pixel pair spacing
DWT: Discrete wavelet transform
G_{RMS}: Root mean square acceleration
ANN: Artificial neural network
CNN: Convolutional neural network
VCPSO: Vibration and communication particle swarm optimization
ANFIS: Adaptive neuro fuzzy inference system
ROI: Region of interest.

Data Availability

The data used to support the findings of this study are included within the article.

Conflicts of Interest

The authors declare that they have no conflicts of interest regarding the publication.

References

[1] J. Mahashar Ali, H. Siddhi Jailani, and M. Murugan, "Surface roughness evaluation of electrical discharge machined surfaces using wavelet transform of speckle line images," *Measurement*, vol. 149, article 107029, 2020.

[2] T. Pfeifer and L. Wiegers, "Reliable tool wear monitoring by optimized image and illumination control in machine vision," *Measurement*, vol. 28, no. 3, pp. 209–218, 2000.

[3] R. K. Shastri and C. P. Mohanty, "Sustainable electrical discharge machining of Nimonic C263 superalloy," *Arabian Journal for Science and Engineering*, vol. 46, no. 8, pp. 7273–7293, 2021.

[4] W. Zhou, X. Li, F. Feng et al., "Robustness of surface roughness against low number of picture elements and its benefit for scaling analysis," *Coatings*, vol. 10, no. 8, p. 776, 2020.

[5] N. A. Hameed, I. M. Ali, and H. K. Hassun, "Calculating surface roughness for a large scale SEM images by mean of image processing," *Energy Procedia*, vol. 157, pp. 84–89, 2019.

[6] T. Jeyapoovan and M. Murugan, "Surface roughness classification using image processing," *Measurement*, vol. 46, no. 7, pp. 2065–2072, 2013.

[7] A. Kumar Parida and K. Maity, "Modeling of machining parameters affecting flank wear and surface roughness in hot turning of Monel-400 using response surface methodology (RSM)," *Measurement*, vol. 137, pp. 375–381, 2019.

[8] S. S. Kumar, M. P. Sudeshkumar, C. Ezilarasan, S. Palani, and J. Veerasundaram, "Modelling and simulation of machining attributes in dry turning of aircraft materials Nimonic C263 using CBN," *Manufacturing Review*, vol. 8, p. 30, 2021.

[9] P. Sivaprakasam and P. Hariharan, "Surface characteristics of nano powder mixed micro-wire electrical discharge machining on Inconel alloy," *Materials Today: Proceedings*, vol. 38, pp. 494–498, 2021.

[10] P. Sivaprakasam, P. Hariharan, and G. Elias, "Experimental investigations on magnetic field-assisted micro-electric discharge machining of Inconel alloy," *International Journal of Ambient Energy*, pp. 1–8, 2020.

[11] S. Dutta, S. K. Pal, S. Mukhopadhyay, and R. Sen, "Application of digital image processing in tool condition monitoring: a review," *CIRP Journal of Manufacturing Science and Technology*, vol. 6, no. 3, pp. 212–232, 2013.

[12] L. Li and Q. An, "An in-depth study of tool wear monitoring technique based on image segmentation and texture analysis," *Measurement*, vol. 79, pp. 44–52, 2016.

[13] H. H. Shahabi and M. M. Ratnam, "Simulation and measurement of surface roughness via grey scale image of tool in finish turning," *Precision Engineering*, vol. 43, pp. 146–153, 2016.

[14] S. Dutta, A. Datta, N. Das Chakladar, S. K. Pal, S. Mukhopadhyay, and R. Sen, "Detection of tool condition from the turned surface images using an accurate grey level co-occurrence technique," *Precision Engineering*, vol. 36, no. 3, pp. 458–466, 2012.

[15] M. Balaji, K. Venkata Rao, N. Mohan Rao, and B. S. N. Murthy, "Optimization of drilling parameters for drilling of TI-6Al-4V based on surface roughness, flank wear and drill vibration," *Measurement*, vol. 114, p. 332, 2018.

[16] S. Dutta, S. K. Pal, and R. Sen, "On-machine tool prediction of flank wear from machined surface images using texture analyses and support vector regression," *Precision Engineering*, vol. 43, pp. 34–42, 2016.

[17] Y. Liu, J. Deng, F. Wu, R. Duan, X. Zhang, and Y. Hou, "Wear resistance of carbide tools with textured flank-face in dry cutting of green alumina ceramics," *Wear*, vol. 372-373, pp. 91–103, 2017.

[18] S. Dutta, S. K. Pal, and R. Sen, "Progressive tool flank wear monitoring by applying discrete wavelet transform on turned surface images," *Measurement*, vol. 77, pp. 388–401, 2016.

[19] J. G. John and N. Arunachalam, "Illumination compensated images for surface roughness evaluation using machine vision in grinding process," *Procedia Manufacturing*, vol. 34, pp. 969–977, 2019.

[20] P. K. Gandla, V. Inturi, S. Kurra, and S. Radhika, "Evaluation of surface roughness in incremental forming using image processing based methods," *Measurement*, vol. 164, article 108055, 2020.

[21] S. M. Ali and N. R. Dhar, "Tool wear and surface roughness prediction using an artificial neural network (ANN) in turning steel under minimum quantity lubrication (MQL)," *World Academy of Science, Engineering and Technology*, vol. 62, pp. 830–839, 2010.

[22] G. Martínez-Arellano, G. Terrazas, and S. Ratchev, "Tool wear classification using time series imaging and deep learning," *International Journal of Advanced Manufacturing Technology*, vol. 104, no. 9–12, pp. 3647–3662, 2019.

[23] H. Chen, A. Chen, L. Xu et al., "A deep learning CNN architecture applied in smart near-infrared analysis of water pollution for agricultural irrigation resources," *Agricultural Water Management*, vol. 240, article 106303, 2020.

[24] A. P. Rifai, H. Aoyama, N. H. Tho, S. Z. Md Dawal, and N. A. Masruroh, "Evaluation of turned and milled surfaces roughness using convolutional neural network," *Measurement*, vol. 161, article 107860, 2020.

[25] Y. He, W. Zhang, Y. F. Li, Y. L. Wang, Y. Wang, and S. L. Wang, "An approach for surface roughness measurement of helical gears based on image segmentation of region of interest," *Measurement*, vol. 183, article 109905, 2021.

[26] L. Xu, C. Huang, C. Li, J. Wang, H. Liu, and X. Wang, "Estimation of tool wear and optimization of cutting parameters based on novel ANFIS-PSO method toward intelligent machining," *Journal of Intelligent Manufacturing*, vol. 32, no. 1, pp. 77–90, 2021.

[27] S. Nouhi and M. Pour, "Prediction of surface roughness of various machining processes by a hybrid algorithm including time series analysis, wavelet transform and multi view embedding," *Measurement*, vol. 184, article 109904, 2021.

[28] J. Xiong, D. Yu, Q. Wang et al., "Application of histogram equalization for image enhancement in corrosion areas," *Shock and Vibration*, vol. 2021, Article ID 8883571, 13 pages, 2021.